Optics & Laser Technology 183 (2025) 112255

Contents lists available at ScienceDirect

Optics and Laser Technology

journal homepage: www.elsevier.com/locate/optlastec

Full length article

Development of an optical fiber surface plasmon resonance sensor decorated with MoS_2/AuNP plasmonic hybrid structure by using polydopamine-assisted electroless plating

Yu Huang [a,b,c,*], Xiaomei Li [a,b,c], Hua Zhang [b,c], Zhiguo Wu [d,f], Rohan Weerasooriya [e], Xing Chen [g], Jiu Zhou [d], Jiangling Wu [h,*], Jianjiang Xue [h], Junbo Wang [b,c], Lei Feng [b,c,*]

[a] Chongqing Jiaotong University, Chongqing 400074, China
[b] Center of Super-Resolution Optics and Chongqing Engineering Research Center of High-Resolution and Three-Dimensional Dynamic Imaging Technology, Chongqing Institute of Green and Intelligent Technology, Chinese Academy of Sciences, Chongqing 400714, China
[c] Chongqing School, University of Chinese Academy of Sciences, Chongqing 400714, China
[d] Wuhan Newfiber Optics Electron Co., LTD, No. 303 Guanggu Avenue, Wuhan East Lake High-tech Development Zone, Wuhan 430075, Hubei Province, China
[e] National Centre for Water Quality Research, National Institute of Fundamental Studies, Hanthana, Kandy 20000, Sri Lanka
[f] Postgraduate Institute of Science, University of Peradeniya, Peradeniya 20400, Sri Lanka
[g] Institute of Industry and Equipment Technology, Hefei University of Technology, Hefei 230009, China
[h] Department of Clinical Laboratory, Medical Sciences Research Center, University-Town Hospital of Chongqing Medical University, Chongqing 401331, China

ARTICLE INFO

Keywords:
Electroless plating
Optical fiber surface plasmon resonance sensor
Molybdenum disulfide
Sensitivity enhancement

ABSTRACT

A simple and low-cost fabrication method via polydopamine accelerated electroless plating (ELP) for an optical fiber surface plasmon resonance (SPR) sensor with molybdenum disulfide nanosheets (MoS_2 NSs) and gold nanoparticles (AuNPs) hybrid structure was proposed. The MoS_2 NSs were prepared by ultrasonic-assisted mixed-solvent liquid-phase exfoliation method. MoS_2 NSs and AuNPs were sequentially immobilized on the optical fiber by electrostatic interaction and Au-S bond supported by polydopamine and 1,2-ethanedithiol respectively, and a gold film supporting SPR was fabricated by ELP to form the optical fiber SPR sensor. The synthesized nanostructures and optical fiber sensors were characterized for their structural, morphological and optical properties. Some key experimental parameters, including dopamine concentration, dopamine polymerization temperature, dopamine polymerization time, pH of MoS_2 NSs solution and plating time, were investigated in detail. The refractive index sensitivity of sensor with the fiber/MoS_2/AuNPs/Au structure achieved 678.85–7231.64 nm/RIU in the range of 1.3329–1.3638, which was approximately 52.35 % and 16.37 % higher than that of conventional sensors in the low refractive index range and high refractive index range respectively. This work proposed a facile, rapid and effective method to fabricate optical fiber SPR sensor to enhance its sensitivity, which indicates the potential application of the fabricated sensor in optical sensing field.

1. Introduction

Surface plasmon resonance (SPR) is the collective oscillations of free electrons that is optically excited at the metal-dielectric interface. The surface plasmon resonance is strongly sensitive to the change of refractive index of surrounding environment adjacent to the metal layer [1]. Thus, this technique of SPR is widely used as an optical biosensor for analyte detection. SPR sensors have been found popular in wide applications for fundamental biological studies, health science research, clinical diagnosis, environmental and agricultural monitoring [2,3]. The conventional Kretschmann configuration is extensively utilized in commercial SPR sensors, but this prism configuration has certain limitations, including large size and complication of optical and mechanical components, which limit their use for miniaturized applications and remote sensing, and reduce its competitiveness in term of cost [1,4]. Compared to the prism based SPR sensor, optical fiber SPR sensors

* Corresponding authors at: Chongqing Jiaotong University, Chongqing 400074, China (Y, Huang). Center of Super-Resolution Optics and Chongqing Engineering Research Center of High-Resolution and Three-Dimensional Dynamic Imaging Technology, Chongqing Institute of Green and Intelligent Technology, Chinese Academy of Sciences, Chongqing 400714, China (L. Feng).
E-mail addresses: huangyu@cigit.ac.cn (Y. Huang), wujiangling@hospital.cqmu.edu.cn (J. Wu), fenglei@cigit.ac.cn (L. Feng).

https://doi.org/10.1016/j.optlastec.2024.112255
Received 28 August 2024; Received in revised form 10 November 2024; Accepted 2 December 2024
0030-3992/© 2024 Elsevier Ltd. All rights are reserved, including those for text and data mining, AI training, and similar technologies.

exhibit numerous excellent benefits, such as simple optical design, portability, cost-effectiveness, and potential for remote sensing, and they are promising biosensing platform for protein and DNA based-assays [5–8]. However, the contents of protein and DNA in bodily fluids are extremely low in early-stage diagnostics. Thus, developing optical fiber SPR sensors with high sensitivity is highly desirable for quantitative analysis.

Modification of the optical fiber structure is a conventional strategy to amplify SPR signal. By using micro/nano processing, such as fused tapering, side polishing, bending into U-shape, more light leaks from fiber core to the external medium, and could enhance the coupling between surface plasmon wave and evanescent field, which is more conducive to the realization of SPR [9,10]. However, these additional fiber processing make the fiber probes extremely fragile and limits their applicability [11]. Recently, due to the advancement of nanomaterial, diverse two-dimensional (2D) atomic layer materials, such as graphene [12], molybdenum disulfide (MoS_2) [13], Mxene [14], have been evaluated as sensing layers to improve the sensitivity of optical fiber SPR sensor. The difference in the work functions between gold and 2D materials layers results in the electrons transfer from 2D material to gold (Au) film under light illumination, which could produce a great enhancement of the electric filed at metal-dielectric interface and improve the detection sensitivity [15]. Wei et al. introduced monolayer graphene synthesized by chemical vapor deposition method on Au coated optical fiber. The refractive index sensitivity of optical fiber sensor with graphene/Au hybrid structure exhibited approximate 2.27-fold improvement compared to traditional optical fiber SPR sensor only coated with Au film [16]. Transition-metal dichalcogenides (TMDC) materials emerge as a promising supplement of graphene have also attracted wide attention in the field of biosensors due to their unique chemical and physical properties. Liu et al. immobilized molybdenum diselenide ($MoSe_2$) layer on Au film coated optical fiber by solution evaporation and demonstrated roughly 98.7 % improvement in the refractive index sensitivity of 2821.81 nm/RIU compared to conventional SPR sensor with Au film only [17]. In comparison to other TMDCs and graphene, MoS_2 has a stronger ability to absorb light and less imaginary part of dielectric constant, which lead it to possess enhanced refractive index sensitivity [18]. Kaushik et al. designed Au coated optical fiber SPR sensor modified with MoS_2 nanosheets (MoS_2 NSs) by dip coating method. The refractive index sensitivity of this developed sensor was improved nearly 2 times compared to conventional one [19]. Wang et al. proposed 4-Amionthiophenol as bridges to connect carboxyl-modified MoS_2 NSs on silver/gold film fabricated on optical fiber [20]. The refractive index sensitivity of the bimetallic optical fiber SPR sensor increased with the increase of MoS_2 layer from one to three layers, and approached maximum sensitivity of 3061 nm/RIU at three layers of MoS_2. Song et al. immobilized MoS_2 NSs on optical fiber core via electrostatic self-assembly before the fabrication of Au film. The refractive index sensitivity of fiber-MoS_2-gold film U-shaped sensor was 6184.4 nm/RIU, which was 25 percent higher than that of sensor with the structure of MoS_2 NSs immobilized on the surface of Au film [21].

Although 2D nanomaterials have proved that they can improve the sensitivity of optical fiber SPR sensor, all essential Au film in the aforementioned studies were prepared by vacuum evaporation or sputtering methods. A uniform thin metal film is necessary to support the excitation of surface plasmon. The existing physical deposition technique requires a specific rotation mechanism tool installed in the chamber to deposit thin metal film on cylindrical fiber core, which increases the fabrication cost of optical fiber sensors and complicates the operation procedure. Electroless plating (ELP) involving the chemical reduction of metal ions in an aqueous solution permits deposition of metals from solution onto surfaces without the need to apply an external electrical potential [22]. This method has been successfully used for the deposition of metals in electronic, aerospace and automotive industries, and the deposition of metals, such as copper, silver, gold and nickel, on solid surfaces to produce fine metallic structure, which is not constrained by shape, size, or conductivity of the supporting substrate [23,24]. Thus, ELP is an appealing method to deposit metal film on the cylindrical surface of fiber core without specific rotation device. The optical fiber SPR sensor using ELP prepared Au films have been reported recently, which shows its high flexibility, cost-effective, relative ease of implementation, compared with Au films prepared by conventional film fabrication technologies [25–27].

Polydopamine (PDA), produced by self-polymerization of its monomer dopamine (DA), is a synthetic melanin analogue with prominent chemical and structural similarities to the native biopolymer [28]. PDA composed of diverse functional groups, such as basic side chain amino groups, the acidic pyrrolecarboxylic functions and the indolic/catecholic π −systems, exhibits excellent adhesion capacity [29]. The strong adhesion property that PDA possess has shown a better efficiency to adsorb gold nanoparticles (AuNPs) on bare optical fiber core in comparison to commonly used 3-aminopropyltrimethoxysilane (APTMS) as the functional adsorption material in ELP [30]. The amion and imion groups of PDA can interact with negatively charged AuNPs via electrostatic interaction, and reduce the time of relative process. Therefore, PDA is more appropriate than APTMS to functionalize the substrate of optical fiber core for the facile, rapid and effective preparation of optical fiber SPR sensors through ELP method.

In this study, we used ELP method to prepare a hybrid structure consisting of MoS_2 NSs and AuNPs (MoS_2/AuNPs structure) interfaced optical fiber SPR sensor. The versatile PDA coating demonstrated a rapid and efficient adsorption capability for MoS_2 NSs and AuNPs via the electrostatic interaction between the amion and imion groups of PDA coating and these negatively charged nanomaterials. The DA polymerization temperature, DA polymerization time, DA concentrations, pH of MoS_2 NSs solvent, plating time were optimized in order to obtain optical fiber SPR sensor with high sensitivity and stability. The experimental results demonstrated that MoS_2/AuNPs structure are able to improve the refractive index sensitivity of optical fiber SPR sensor at least 16 % compared to the conventional counterpart without using this hybrid structure, which show broad application prospects in fields of biosensor.

2. Experimental section

2.1. Material and reagents

Dopamine hydrochloride, 1,2-ethanedithiol, ethanol and MoS_2 powder (98 %) were purchased from Aladdin (Shanghai, China).Trichlorogold hydrate hydrochloride ($HAuCl_4{\cdot}3H_2O$) came from Sigma-Aldrich (Merck, Darmstadt, Germany). Sodium citrate tribasic hydrate, hydroxylammonium chloride (98.5 %) and Tris (hydroxymethyl) aminomethane were ordered from Macklin (Shanghai, China). Other reagents used in this study were obtained as analytical reagent grade. All solutions were prepared using ultrapure water (18.25 MΩ·cm). Multimode optical fiber with a 600 μm core diameter and 0.37 numerical aperture were purchased from Nanjing Chunhui Science Technology Industrial Co., Ltd.

2.2. Apparatus

The optical fiber SPR sensor platform had been used previously as shown in Fig. S1. A bifurcated optical fiber coupler was used to deliver light from the tungsten halogen lamp to the optical fiber SPR sensor, and then collected the reflected light from the fiber probe to the spectrometer (EQ2000, Choptics Co., Ltd, Shanghai, China). The ultrasonic homogenizer (Ymnl-1000 T, Nanjing YMNL Instrument and Equipment Co., Ltd, China) was employed to fabricate MoS_2 NSs. Absorbance measurement was carried out using a custom-made absorption spectrometer [31]. Raman spectroscopy was performed using an InVia Raman microscope (Renishaw) at excitation laser wavelength of 532 nm. The morphologies of MoS_2 NSs and AuNPs were observed using a T-20 transmission electron microscope (TEM, FEI, USA). Hydrodynamic

size distribution and zeta potential were measured on a Malvern Zetasizer Nano ZS analyzer. The surface of optical fiber SPR sensor and its cross-section were characterized by scanning electron microscopy (Hitachi SU8010) equipped with a Horiba EX 350i energy dispersion spectrometer (EDS) operated at 3.0 kV at a 3.2–4.8 mm working distance under the vacuum less than 1×10^{-3} Pa. The surface profile of the optical fiber SPR sensor was also characterized by a AFM (Bruker, Dimension FastScan/Icon, Germany) in an intelligent image mode at a 0.98 HZ scan rate with the type of scanasyst-air probe and a 256 × 256 pixel resolution under conditions of relative humidity of 65 % at temperature of 25 ℃. An Abbe's refractometer (Shanghai Optical Instrument Plant, China) was used to measure the refractive index of solutions.

2.3. Synthesis of gold nanoparticles

AuNPs with diameter of approximately 12 nm were synthesized based on the standard citrate reduction procedure. In brief, 100 mL of 1 mM hydrate hydrochloride was heated to boiling. Then, 15 mL of 1 % trisodium citrate solution was rapidly added to $HAuCl_4$ solution quickly under vigorous stirring. The solution was kept boiling for 20 min and was then allowed to cool down naturally to room temperature. The product was filtered by 0.22 μm PES Syringe Filers and stored in a dark glass bottle cleaned by aqua regia at 4 ℃. The concentration of AuNPs was spectrometrically estimated as 8 nM based on the Lambert-Beer Law [32].

2.4. Synthesis of MoS_2 nanosheets

MoS_2 NSs were prepared by ultrasonic-assisted mixed-solvent liquid-phase exfoliation method referring to the previous work [33]. MoS_2 powder of 1500 mg was added to 250 mL ethanol/water mixture with ethanol volume fraction of 45 % (v/v, denoting as 45 %). Then, the sealed beaker containing the above mixture was ultrasonicated at 40 % amplitude for 20 h with 5 s/5 s on/off pulse ratio at 15 ℃. The produced dark green suspension was centrifuged at 8000 rpm for 30 min at three times in order to remove bulk MoS_2. The yellow-green supernatant containing MoS_2 NSs was collected and stored at 4 ℃ as the stock solution. The concentration of MoS_2 NSs in the dispersion was estimated as ~ 200 mg/L.

2.5. ELP preparation of optical fiber SPR sensor with fiber/MoS_2/AuNPs/Au structure

The optical fibers were cut to a length of 20 cm, and the jacket and polymer-cladding were removed over an area of 5 mm for sensing. The MoS_2/AuNPs hybrid structure was assembled and Au film was formed on the optical fiber in the following steps. Step 1: Cleaning. The uncladded core of the optical fiber was treated with a piranha solution (7:3 mixture of concentrated H_2SO_4 and 30 % H_2O_2) for 30 min at 90 ℃. The piranha-cleaned fiber was thoroughly rinsed with ultrapure water and subsequently dried at 70 °C oven for 1 h. Step 2: Polymerizaition of the first PDA layer. The cleaned optical fiber core was functionalized through a DA polymerization reaction by immersion in freshly prepared DA solution (5 mg/mL in 10 mM Tris-HCl, pH 8.5) under stirring of 450 rpm at 10 ℃ for 15 min. DA was spontaneously polymerized to PDA in this oxidative environment and the PDA was formed as a layer (denoted as PDA-1) at the optical fiber core surface. After rinsing with ultrapure water, the optical fiber was placed inside the oven for 30 min at 70 °C again. Step 3: Adsorption of the MoS_2 NSs. This PDA-functionalized optical fiber was immersed in the MoS_2 NSs solution (pH 3) for 5 h to absorb MoS_2 NSs onto the PDA-1 surface due to the electrostatic effect between the positively charged amino and imino groups of PDA and negatively charged MoS_2 NSs, and dried in an oven at 60 °C for 30 min. Step 4: Thiol-functionalization of MoS_2 NSs. To attach AuNPs on MoS_2 NSs, the surfaces of MoS_2 NSs were modified with thiols. The optical fiber immobilized with MoS_2 NSs was immersed in 1,2-ethanedithiol solution in ethanol (10 mM) for 5 min followed by rinsing with abundant ethanol and drying in oven. Step 5: Adsorption of AuNPs. The 1,2-ethanedithiol-covered optical fiber was then submerged in AuNPs colloids (8 nM) for 5 min followed by rinsed by ultrapure water. The citrate-capped AuNPs were bound to the thiol-functionalized MoS_2 NSs, forming the MoS_2/AuNPs hybrid structure. By repeating the above steps in 5 cycles, a layer of AuNPs was formed on the surface of MoS_2 NSs. Step 6: Polymerizaition of the second PDA layer. Subsequently, this optical fiber was immersed in an aqueous solution of DA (0.5 mg/mL in 10 mM Tris-HCl, pH 8.5) under stirring at 450 rpm for 15 min at 10 ℃ to form a second PDA layer (denoted as PDA-2), and then rinsed with ultrapure water and placed in an over at 70 ℃ for 30 min. Step 7: Adsorption of AuNPs as seeds. Afterward, AuNPs were adsorbed onto the PDA-2 layer functionalized surface by immersing the optical fiber in the AuNPs colloid for 3 h. The optical fiber with immobilized AuNPs was rinsed with ultrapure water, dried in oven, and immediately used in the ELP. Step 8: ELP. Finally, the optical fiber core adsorbed with AuNPs was immersed in a mixture of 0.05 % $HAuCl_4$ and 0.2 mM $NH_2OH{\cdot}HCl$ at 540 rpm for 10 min to form a continuous Au film at the cylindrical and end surface of optical fiber core simultaneously. After washing by ultrapure water and drying, the optical fiber SPR probe was ready for use. The sensing performance of these fabricated optical fiber probes were determined using the custom-made optical fiber SPR sensor platform. The preparation process of the electroless-plated Au film for optical fiber SPR sensor with this structure is shown in Fig. 1.

2.6. ELP preparation of optical fiber SPR sensor with fiber/Au structure

The procedure to fabricate the optical fiber SPR sensor with fiber/Au structure is adapted and simplified from that of sensor with fiber/MoS_2/AuNPs/Au structure. Briefly, the multimode optical fiber with unclad portion was cleaned with piranha solution and dried in oven. This processed fiber was then vertically dipped in freshly prepared DA solution (5 mg/mL in 10 mM Tris-HCl, pH 8.5) under stirring of 450 rpm at 10 ℃ for 15 min to coat PDA layer on the fiber core and placed into AuNPs solution for 3 h to adsorb AuNPs on this PDA layer sequentially. Finally, the fiber probe was kept in the mixture of 0.05 % $HAuCl_4$ and 0.2 mM $NH_2OH{\cdot}HCl$ at 540 rpm for 7.5 min to form Au film on its surface. After being rinsed with a large amount of ultrapure water, the fiber probe was dried at 70 ℃ before use.

2.7. Refractive index sensitivity of the optical fiber SPR sensor

The ethanol/water mixture with ethanol volume fraction of 0 %, 10 %, 20 %, 30 %, 40 %, 50 %, 60 %, 70 %, 80 %, with corresponding refractive index of 1.3329、1.3381、1.3442、1.3501、1.3552、1.3588、1.3613、1.3629、1.3638, were prepared. The optical fiber sensor probe was immersed in the solution with different refractive index during each measurement. The refractive index sensitivity is defined as:

$$S_{n\_res} = \delta\lambda_{res}/\delta n \quad (1)$$

where $\delta\lambda_{res}$ represents the shift in corresponding resonance wavelength and δn is the change in the refractive index of ethanol/water mixture.

3. Results and discussion

3.1. Characterization of gold nanoparticles and MoS_2 nanosheets

The absorbance spectra of AuNPs and MoS_2 NSs were measured as shown in Fig. 2a and b. The AuNPs exhibited a characteristic resonance peak at ~ 520 nm due to their localized surface plasmon resonance. The spectrum obtained from exfoliated MoS_2 NSs showed prominent peaks at 667 nm (A-exciton) and 610 nm (B-exciton) respectively, which are assigned to the direct excitonic transitions of MoS_2 at the K point of the

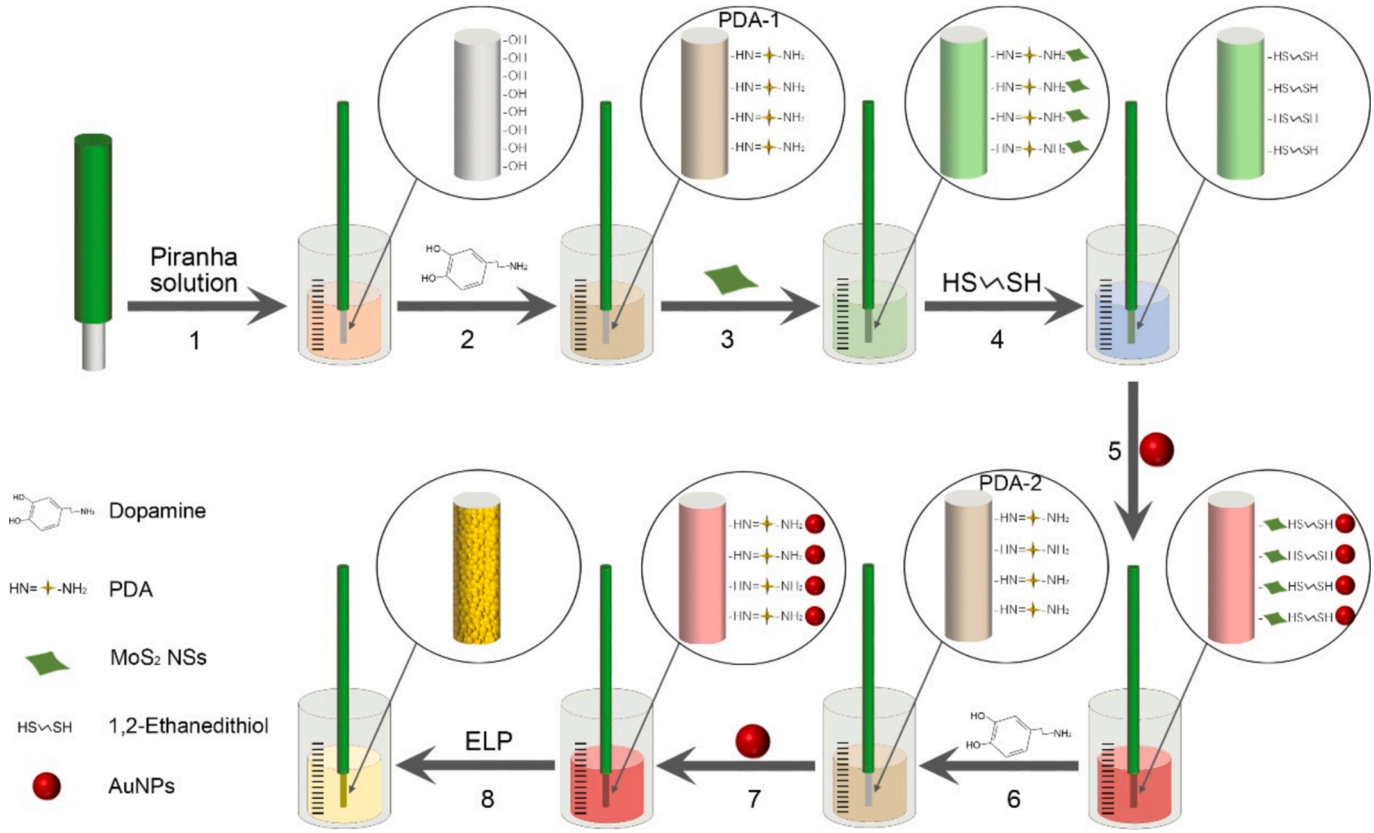

Fig. 1. Schematic illustration of the ELP fabrication of optical fiber sensor with fiber/MoS_2/AuNPs/Au structure.

Brillouin zone [34]. TEM characterizations were performed on AuNPs and MoS_2 NSs to analyze their quality and dimensions. As exhibited in Fig. 2c, the AuNPs synthesized by this citrate reduction method had the spherical shape with about 12 nm diameter and well monodispersed. The exfoliated MoS_2 NSs displayed a typical layered nanostructure with the wrinkle and crumple (Fig. 2d). Dynamic light scattering (DLS) measurements were also performed to determine the hydrodynamic radius of AuNPs and MoS_2 NSs (Fig. 2e). The size distribution of AuNPs showed only one peak, which means the hydrodynamic diameter of AuNPs was about 12 nm. The layered MoS_2 NSs prepared from the sonication-assisted exfoliation technique had various plane sizes in the range from 45 nm to 950 nm, with a majority at 340 nm. Moreover, Raman spectroscopy was applied to further confirm the nature of MoS_2 NSs. Fig. 1f shows Raman spectra of MoS_2 NSs excited at 532 nm. There were two characteristic peaks of 379.7 and 404.3 cm^{-1}, which are assigned to the in-plane (E_{2g}) and out-of-plane (A_{1g}) lattice vibrations respectively [35]. The A_{1g}-E_{2g} Raman shift can be used to distinguish layered MoS_2 NSs and its counterpart of bulk MoS_2 [36]. A frequency difference of 26.5 cm^{-1} was observed for bulk MoS_2, while this value was decreased to 24.6 cm^{-1} for MoS_2 NSs, which is consistent with previous literature reports [19,36]. All these physicochemical characterization results confirm the successful preparation of AuNPs and layered MoS_2 NSs.

3.2. Optimization of optical fiber SPR sensor with fiber/Au structure fabrication procedure

The thickness of Au film coated on optical fiber core is important since the approximately 40–60 nm thickness is able to excite the surface plasmon resonance [25]. Furthermore, in the PDA accelerated ELP process, three factors including DA concentration, DA polymerization time and DA polymerization temperature are assumed to affect the polymerization rate and polymerization degree, and govern the formation of PDA layer, which are important to adsorb AuNPs as seeds to prepare the ELP. Thus, the effects of DA concentration, DA polymerization time and DA polymerization temperature were first evaluated followed by plating time to optimize the fabrication of optical fiber SPR sensor with fiber/Au structure, at a certain concentration of 0.05 % $HAuCl_4$ and 0.2 mM $NH_2OH{\cdot}HCl$ to form Au film on the fiber core, which had been determined by our group previously [27]. DA polymerization temperature, DA polymerization time and plating time were maintained as 15 ℃, 15 min and 7.5 min respectively here. To evaluate the sensitivity of the prepared sensor to the surrounding refractive index, the sensor was immersed in various ethanol/water mixture with varying refractive indices ranging from 1.3329 to 1.3638. The reflection spectra of sensors prepared under DA concentration of 1, 3, 5, 7, 9 mg/mL in solvents with different refractive indices were determined as shown in Fig. 3. The resonance wavelength of sensors generated by DA concentration of 3, 5, 7, 9 mg/mL measured at the solvent with the refractive index of 1.3329 were at 659.05 nm, 665.54 nm, 660.15 nm and 670.59 nm respectively. All reflection spectra shown red shifts of approximately 57.98–64.77 nm as the refractive index of solution increased to be 1.3638. Notably, the reflection spectra of sensor prepared by 1 mg/mL of DA concentration was broad and tortuous, its refractive index sensitivity and FWHM were not evaluated. The resonance wavelength λ_{res} of these sensors had a nonlinear relationship with refractive index n, which can be expressed as follows:

$$\lambda_{res} = \mathrm{a} \times e^{(b \times \mathrm{n})} \quad (2)$$

where a and b represent the fitting parameters.

The relationship between the resonance wavelength of sensors prepared by DA concentration of 3, 5, 7, 9 mg/mL and the refractive index of solutions is shown in Fig. 4. A comparison of their refractive index sensitivities and full width at half maximum (FWHM) is presented in Table S1. Increasing DA concentration would decrease the refractive

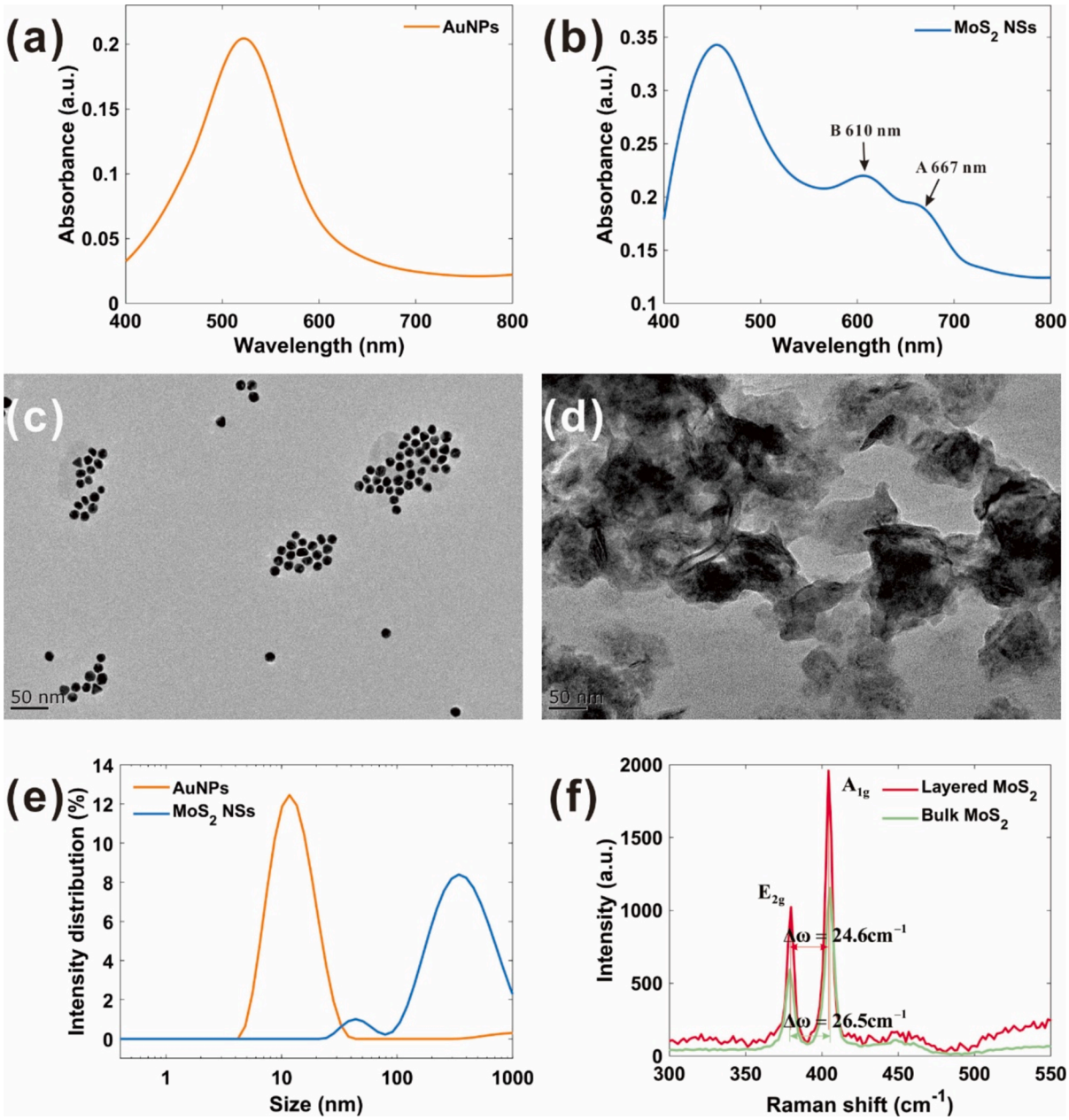

Fig. 2. Absorption spectra of (a) AuNPs and (b) layered MoS_2 NSs. TEM micrographs of (c) AuNPs and (d) MoS_2 NSs. (e) DLS spectra of AuNPs and MoS_2 NSs. (f) Raman spectra of bulk MoS_2 and MoS_2 NSs.

index sensitivity at low refractive index range but reverse this trend at high refractive index range. The sensor fabricated by DA concentration of 5 mg/mL had a comparable refractive index sensitivity in all refractive index range while maintained a smallest FWHM and largest shift of resonance wavelength in this refractive index range. These results shown that 5 mg/mL was the optimal DA concentration for the preparation of optical fiber SPR sensors.

To evaluate the effect of DA polymerization time, DA concentration, DA polymerization temperature and plating time were maintained as 5 mg/mL, 15 ℃ and 7.5 min respectively. DA polymerization time of 10, 15 and 20 min were used to fabricate the optical fiber sensor. The SEM images of PDA surface prepared at these polymerization time, the plot of resonance wavelength changed with refractive index, and the refractive index sensitivity and FWHM of these sensors prepared under these conditions are shown in Fig. S2 and Table S2. As shown in Fig. S2 a, d and g, the thickness of PDA layer increased with the DA polymerization time from 8.71 to 17.74 nm. The color of reaction solution produced by different DA polymerization time became darker with the increase of polymerization time, which confirms that longer polymerization time would produce larger particle (Fig. S3). The corresponding refractive index sensitivity and FWHM of these prepared sensors increased first and then decreased with the increase of DA polymerization time. Thus, the sensor prepared with DA polymerization time of 15 min was determined as the optimal time for the preparation of PDA layer.

DA polymerization temperature is another parameter needed to be determined since the proper reaction temperature could also affect the deposition of PDA layer [25]. 5,10,15 and 20 ℃ were used as the temperature to polymerize DA while the DA polymerization time, DA concentration and plating time were maintained as 15 min, 5 mg/mL and 7.5 min respectively. The photographs of solutions after polymerization were obtained as shown in Fig. S4. The solution experienced higher temperature shown darker color, which indicates that higher DA polymerization temperature resulted in larger particles in the reaction system. As illustrated in Fig. S5, the resonance wavelength of all optical

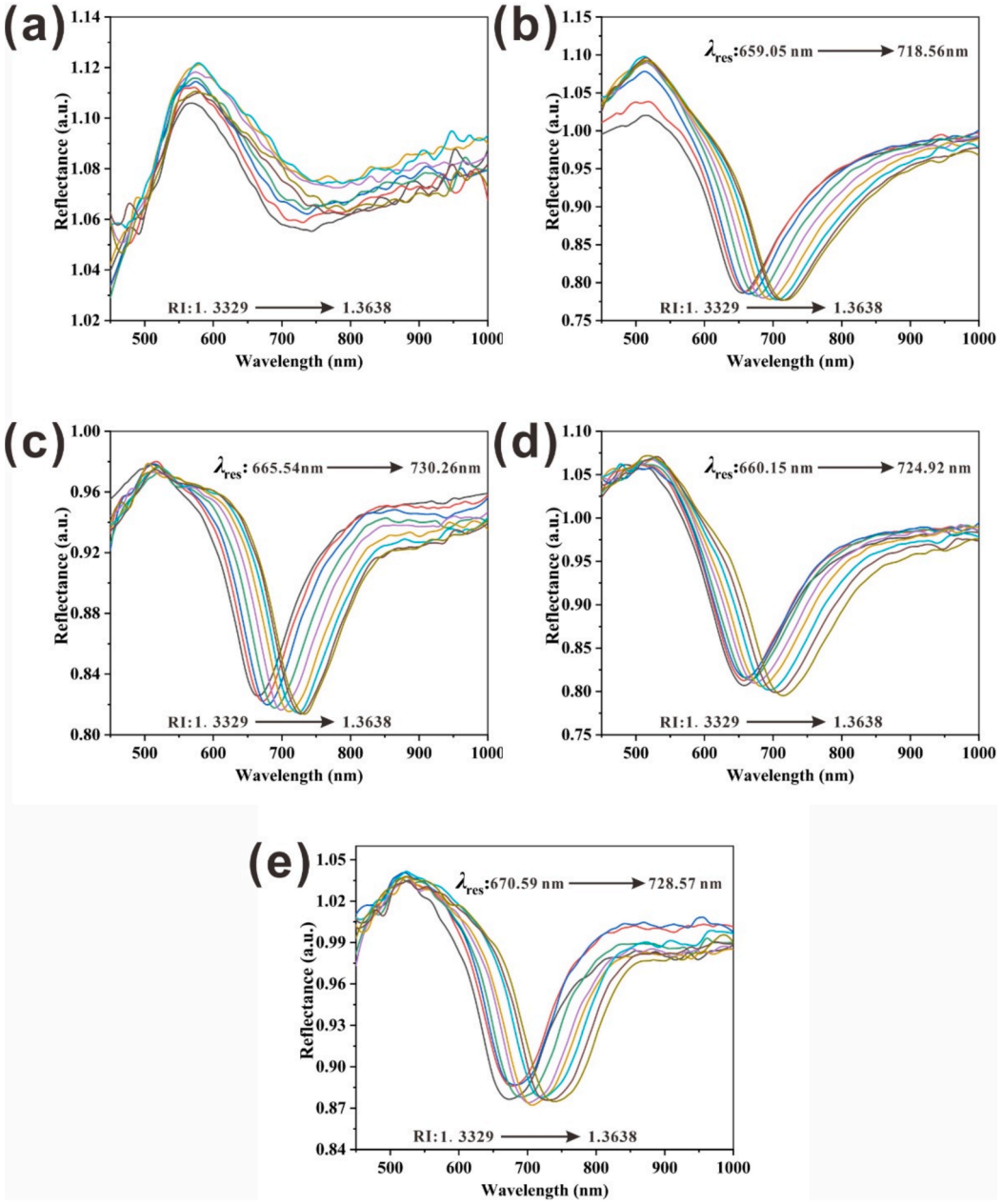

Fig. 3. Reflection spectra of optical fibers with fiber/Au structure fabricated by DA concentration of (a) 1, (b) 3, (c) 5, (d) 7 and (e) 9 mg/mL in solvents with different refractive index (RI) values.

fiber probes produced by DA polymerization temperature of 5, 10, 15 and 20 ℃ redshifted with the ascending refractive index of solution. Their refractive index sensitivity was evaluated and illustrated in Fig. S5 b, d, f and h. The spectral analysis showed that the relationship between resonance wavelength shift and solution refractive index was consistent with an exponential fit, and in the range between 329.89 and 5977.4 nm/RIU. The refractive index sensitivity at low refractive index range exhibited an increase with an increasing refractive index while it approached the highest point at 10 ℃ (Table S3). Moreover, taking the FWHM and $\Delta\lambda_{\_max}$ into consideration, optical fiber probes produced by DA polymerization temperature of 10 and 15 ℃ had a better value in comparison to two other counterparts, while the sensor produced at 10 ℃ had the narrowest FWHM and largest shift in resonance wavelength, the polymerization temperature of 10 ℃ was then chosen in the following sensor fabrication process.

An approximately thickness of Au film is important to excite SPR. Therefore, the control of the thickness of Au film by governing the plating time was carried out. Varying the plating time is the most effective strategy to control the thickness of Au thin film deposited on the core of an optical fiber. To assess the effect of plating time on the sensing performance, DA concentration of 5 mg/mL, DA polymerization time of 15 min, DA polymerization temperature of 10 ℃ were maintained while the plating time was varied as 5, 7.5, 10, 12.5 min respectively. Fig. S6 a, c, e and g shown that the resonance wavelength of optical fiber gradually increased with increasing plating time because the Au film became thicker. As shown in Fig. S6 b, d, f, h and Table S4, the refractive index sensitivity and maximum change of resonance wavelength monotonically increased as the plating time increased, and the FWHM decreased first and then increased dramatically. The refractive index sensitivity and maximum change of resonance wavelength were relatively high and the FWHM was relatively narrow for the optical fiber sensor when the plating time was 10 min. Then, 10 min was

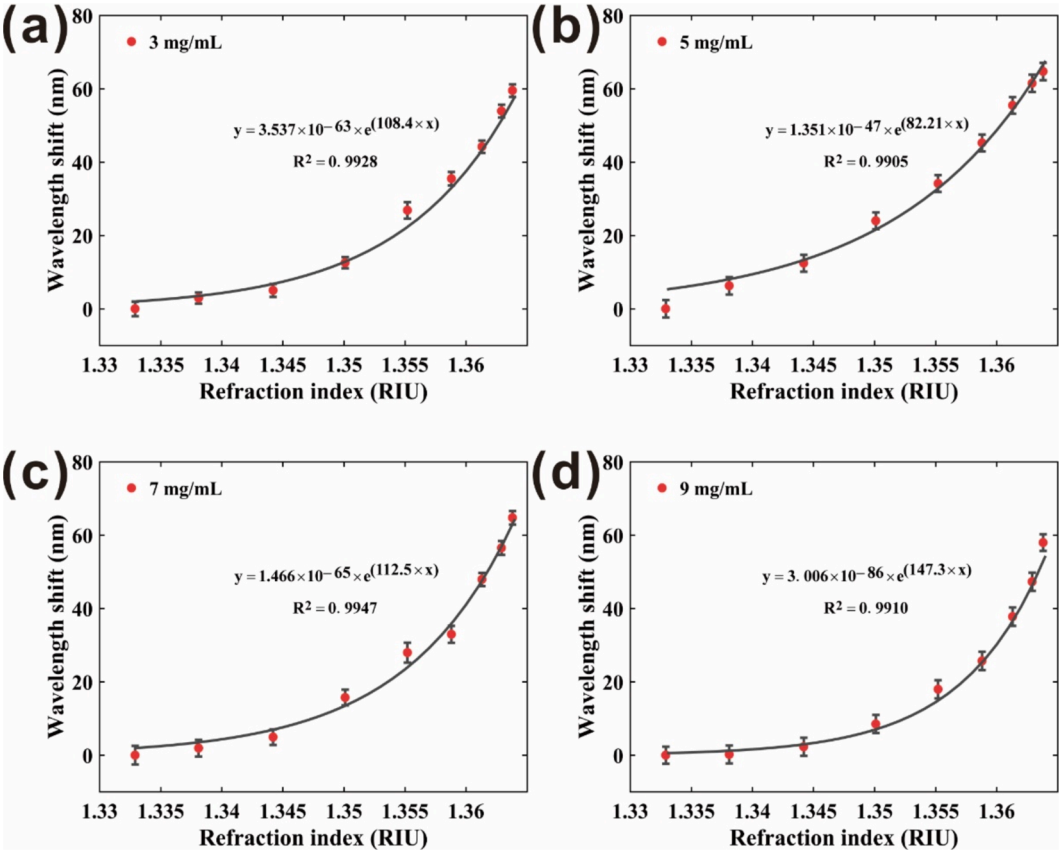

Fig. 4. Fitting curves of relationship between resonance wavelength shift (compared with RI:1.3329) of sensors fabricated by DA concentration of (a) 3, (b) 5, (c) 7 and (d) 9 mg/mL and refractive index.

the optimized plating time for the preparation of optical fiber SPR sensor with fiber/Au structure.

3.3. Characterization of optical fiber SPR sensor with fiber/Au structure

Surface, cross-sectional SEM images, AFM images were acquired to characterize the morphology and thickness of Au film of optical fiber sensors produced by the above-mentioned optimal parameters. Fig. 5a, b and c show the surface and cross-section SEM images of the electroless-plated Au film. A relatively continuous and uniform Au film were absorbed on the optical fiber with a thickness of 54.03 ± 3.19 nm. The EDS measurement of this Au-coated optical fiber indicates that this probe was composed of the element Au, Si and O (Fig. 5d). The AFM testing was selected to observe the surface morphology of Au film (Fig. 5e and f). The Au film showed a relatively flat surface with a surface roughness of 5.00 nm.

3.4. Optimization of optical fiber SPR sensor with fiber/MoS_2/AuNPs/Au structure fabrication procedure

The fabrication procedure of optical fiber SPR sensor only with Au film has been optimized as mentioned-above. The immobilization of additional MoS_2 NSs and AuNPs is expected to improve the performance of optical fiber SPR sensor. A PDA-1 layer is designed to form on the fiber core to absorb MoS_2 NSs due its excellent adhesion capability. Sulfur vacancies presented in these liquid exfoliated MoS_2 NSs could be functionalized via thiol conjugation[37]. Then, 1,2-ethanedithiol acts as bridges to link MoS_2 NSs absorbed on the fiber core through their edged site or defective sites at its one end and AuNPs by Au-S chemical bond at its other end. When the MoS_2 NSs and AuNPs have been sequentially immobilized on optical fiber, the PDA-2 layer is formed on the basis of MoS_2/AuNPs structure to absorb additional AuNPs on its surface and perform ELP. PDA has abundant pH-dependent amion and imine groups of poly(catecholamine), which are positively charged under acidic condition and suitable to absorb negatively charged nanomaterials. The parameters to fabricate PDA layers of sensor with fiber/Au structure could be used here for fabrication of PDA-1 layer. Due to more significant influence of DA concentration on the formation of PDA layer than other parameters related to the PDA layer fabrication, thus, the pH of MoS_2 NSs solution, DA concentration for fabrication of PDA-2 layer, and plating time were evaluated to optimize the fabrication of optical fiber SPR sensor with fiber/MoS_2/AuNPs/Au structure. DA polymerization time of 15 min and DA polymerization temperature of 10 ℃ were maintained for fabrication of PDA-2 layer.

The pH of synthesized MoS_2 NSs solution was approximately 3, which is significantly lower than the pKa values of amion and imine groups (10.6 and 17 respectively) of the PDA layer [30]. The amion and imine groups supplied by the PDA layers were protonated and positively charged in this MoS_2 NSs solution, which is preferred to interact with negatively charged MoS_2 NSs via the electrostatic interaction. The optical fiber immobilized with MoS_2 NSs exhibited light yellow as shown in Fig. 6a. The use of 1,2-ethanedithiol is able to link both MoS_2 NSs and AuNPs via thiol conjugation to produce MoS_2/AuNPs hybrid structure on the optical fiber, which exhibited red color as shown in Fig. 6b. Fig. 6c displays the Raman spectra of MoS_2 NSs and Au decorated MoS_2 NSs. After AuNPs incorporation, the downshift of both the A_{1g} and E_{2g} suggests that the Au NPs acts as n-type dopant and the result is consistent with previous reports [38,39]. Upon decoration of pristine MoS_2 NSs with AuNPs, the increase in Raman mode intensity is due to the enhanced localized electromagnetic field in the vicinity of AuNPs. The morphological characterization of optical fiber with immobilization of MoS_2 NSs and MoS_2/AuNPs structure was studied by TEM analysis as

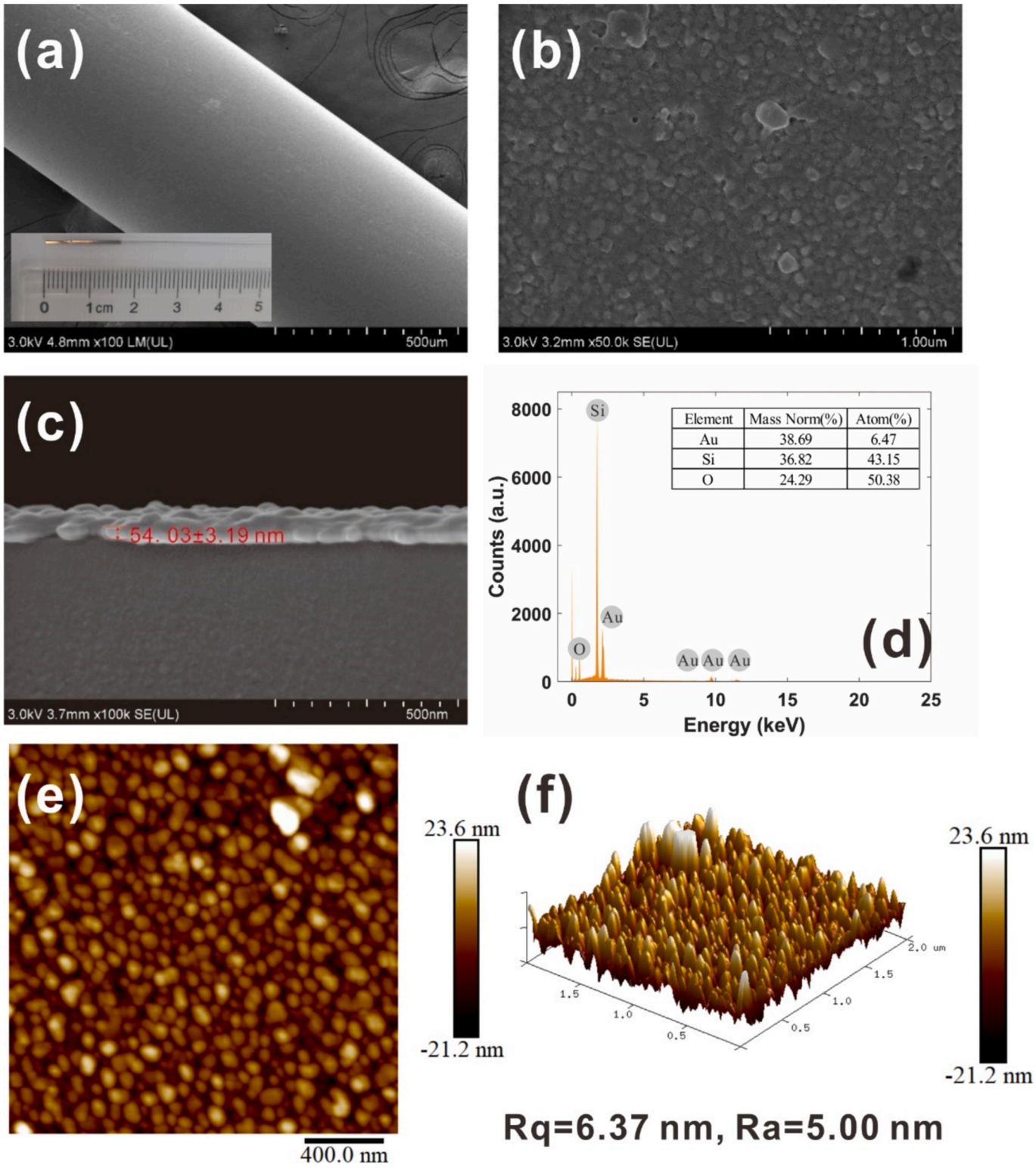

Fig. 5. SEM images of (a) top view, (b) surface morphology, (c) cross section of electroless-plated Au film coated optical fiber probe with fiber/Au structure. The inset in (a) is the photograph of the optical fiber SPR sensor. (d) The EDS spectrum of optical fiber probe with fiber/Au structure. (e, f) AFM images of electroless-plated Au film. Two profile roughness parameters, including roughness average (Ra), RMS roughness (Rq), were labeled at the bottom.

depicted in Fig. 6d and e respectively. The surface modification was apparent. Then the effect of pH in MoS_2 NSs solution to fabricate the optical fiber SPR sensor with fiber/MoS_2/AuNPs/Au structure was first evaluated for optimization while the DA concentration and plating time were maintained as 5 mg/mL and 10 min respectively. As illustrated in Table S5, the zeta potential of MoS_2 NSs were all negatively charged within a pH range of 2–5. Apparent zeta potential of MoS_2 NSs measured at pH of 2–4 were similar to each other, but the zeta potential of MoS_2 NSs at pH of 5 was significantly reduced, indicating good colloidal stability in aqueous dispersion. As shown in Fig. S7 and Table S5, the corresponding refractive index sensitivity of sensors in the low and high refractive index range, $\Delta\lambda_{max}$, increased first and then descended with

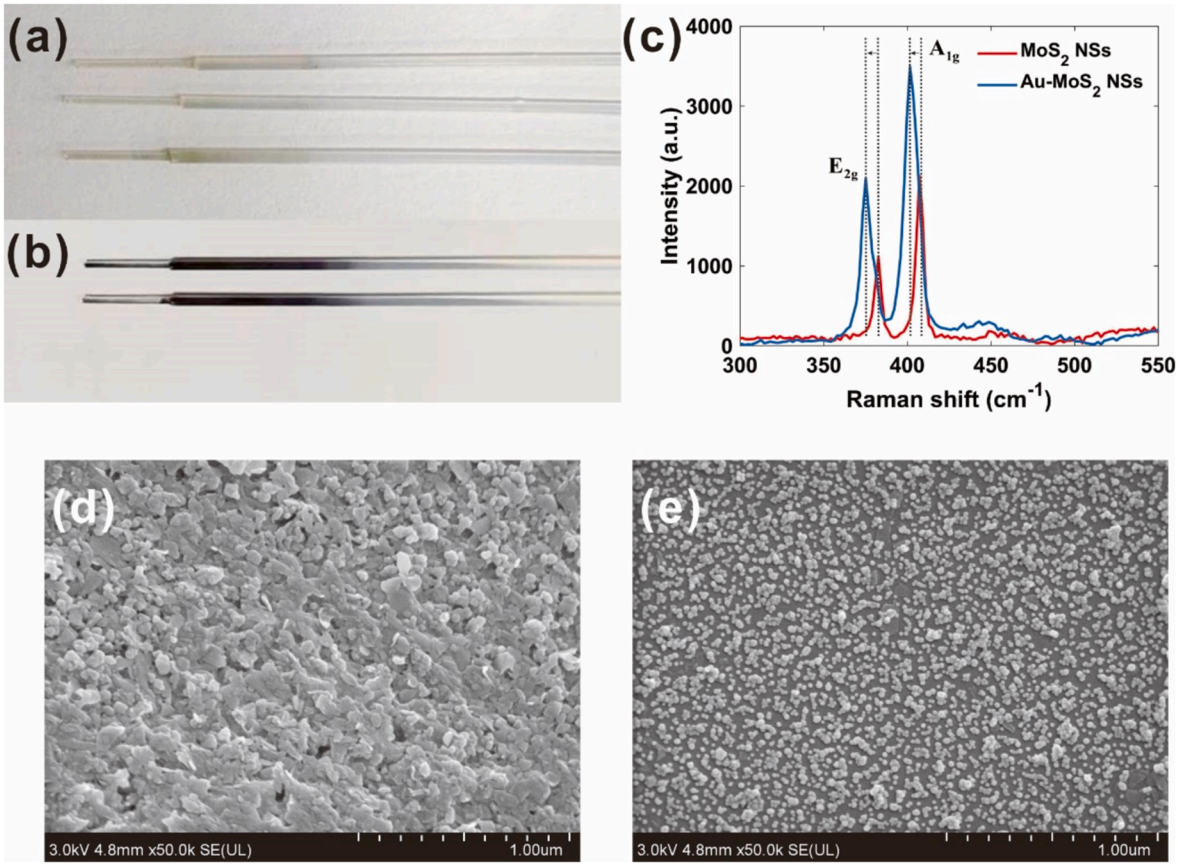

Fig. 6. Fabrication of MoS_2/AuNPs structure. Photographs of optical fiber immobilized with (a) MoS_2 NSs and (b) MoS_2/AuNPs structure respectively. (c) Raman spectra of layered MoS_2 and MoS_2/AuNPs structure. TEM images of optical fiber immobilized with (d) MoS_2 NSs and (e) MoS_2/AuNPs structure.

ascending pH of MoS_2 NSs solution while the FWHM had a reversed trend. From the data obtained in this study, MoS_2 NSs solution with pH of 3 was selected as the optimal pH in solution.

The parameters of DA concentration to fabricate the PDA-2 layer and plating time to implement ELP to form Au film were optimized successively to fabricate the sensor with fiber/MoS_2/AuNPs/Au structure. As shown in Fig. S8 and Table S6, the refractive index sensitivity and maximum change in resonance wavelength monotonically decreased but the FWHM increased with increasing DA concentration, so 0.5 mg/mL of DA concentration was selected for fabrication of PDA-2 layer. The plating time dependent of the performance of sensor was shown in Fig. S9 and Table S7. The refractive index sensitivity in low refractive index range first increased and then decreased with the plating time increasing from 5 to 12.5 min. However, the refractive index sensitivity in high refractive index range had a reversed trend. The FWHM of sensor produced by 10 min had the narrowest while others were larger than 150. Therefore, the optimal plating time was 10 min. Then, DA concentration of 0.5 mg/mL, DA polymerization time of 15 min, DA polymerization temperature of 10 ℃ were determined to fabricate the PDA-2 layer and the plating time was selected as 10 min.

3.5. Characterization of optical fiber SPR sensor with fiber/MoS_2/AuNPs/Au structure

SEM and AFM measurement were performed to analyze the surface and cross section of Au film of optical fiber sensors with fiber/MoS_2/AuNPs/Au structure produced by optimized parameters. As shown in Fig. 7a, b and c, a compact and uniform Au film with a thickness of about 62.13 nm was produced on the surface of optical fiber. MoS_2 NSs and AuNPs were integrated well in Au film and cannot be distinguished separately. To probe the elemental composition, EDS elemental analysis of probe with characteristics peaks of Au, Mo and S is shown in Fig. 7d. AFM analysis illustrated in Fig. 7e and f clearly depicts a relatively flat surface of Au film with a surface roughness of 4.58 nm presented on the optical fiber.

3.6. Bulk refractive index test

The refractive index test explored the sensing properties of the optical fiber SPR sensor with fiber/Au structure and fiber/MoS_2/AuNPs/Au structure respectively. The refractive index experimental resonance spectra and their sensitivity fitting curves are shown in Fig. 8. The refractive index range of ethanol/water mixture used in the experiment was 1.3329–1.3638. The sensitivity of sensor with fiber/Au structure is 445.38–6214.31 nm/RIU and linearity 0.9915. The sensitivity of sensor with fiber/MoS_2/AuNPs/Au structure is 678.85–7231.64 nm/RIU and linearity 0.9883. The fiber probe with MoS_2/AuNPs structure on its surface exhibited significant improvement in the sensitivity. Furthermore, the sensitivity of these sensors in high refractive index range is obviously higher than that in the low refractive index range, which is ascribed to an increase in the electric field penetration depth and a long propagation distance of surface plasmon polaritons. When the refractive index of the surrounding environment is increased to nearly match that of the optical fiber core, a symmetric plasmonic resonance excitation configuration is generated on both sides of the Au film, which produces a lower attenuation of surface plasmon polaritons and enhances their electric filed intensity [40,41]. From the experimental data, it is observed that the resonance wavelength of sensor with fiber/MoS_2/AuNPs/Au structure is red-shifted compared to that sensor without MoS_2 /AuNPs structure, and the sensitivity is improved by at least 200 nm/RIU with respect to its counterpart. The performance of these sensors proposed in this work is compared with previous work. As

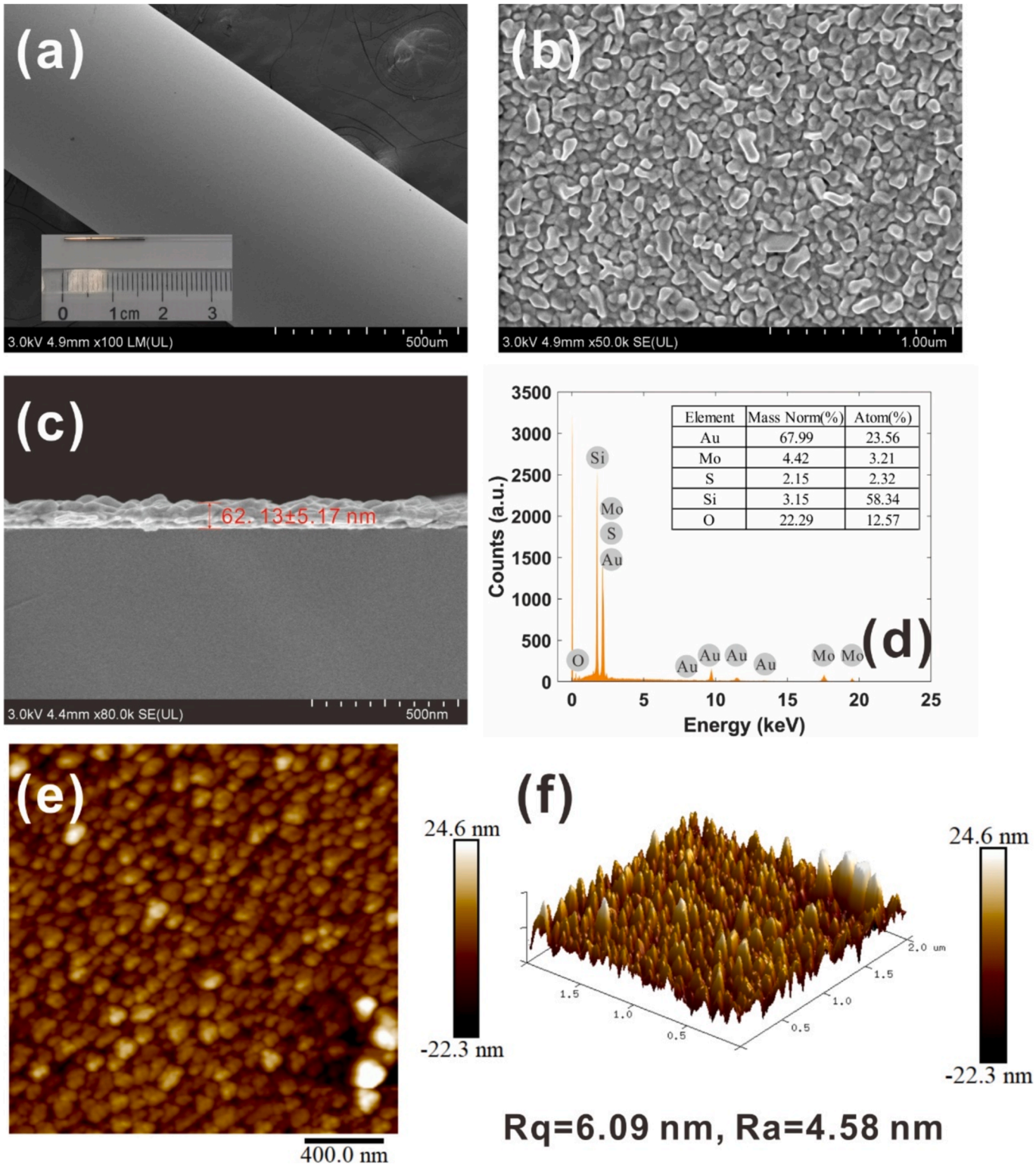

Fig. 7. SEM images of (a) top view, (b) surface morphology, (c) cross section of electroless-plated Au film coated optical fiber probe with fiber/MoS_2/AuNPs/Au structure. The inset in (a) is the photograph of the optical fiber SPR sensor. (d) The EDS spectrum of optical fiber probe with fiber/MoS_2/AuNPs/Au structure. (e, f) AFM images of electroless-plated Au film. Two profile roughness parameters, including roughness average (Ra), RMS roughness (Rq), were labeled at the bottom.

illustrated in Table 1, this optical fiber SPR probes established in this study had a comparable sensitivity, simple structure and low-cost in fabrication.

3.7. Repeatability of the optical fiber sensors

The repeatability of the optical fiber SPR sensors with fiber/Au structure and fiber/MoS_2/AuNPs/Au structure was measured via the consistency of the results obtained from detecting the pure water. Tables S8 and S9 compared the resonance wavelength, the maximum

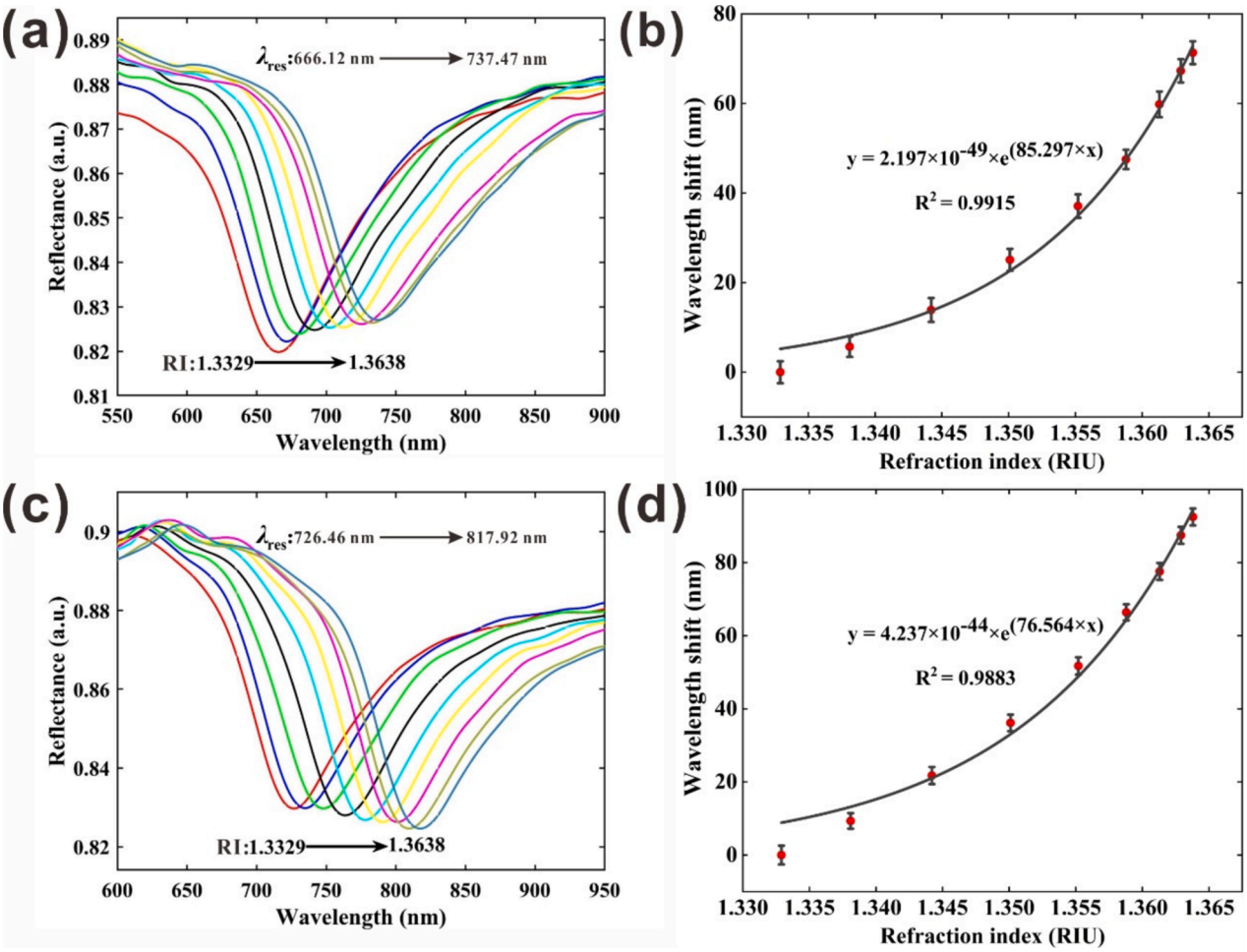

Fig. 8. Spectra of optical fiber SPR senor with fiber/Au structure in solvents with different RI values (a) and refractive index sensitivity fitting curve (b). Spectra of optical fiber SPR senor with fiber/MoS_2/AuNPs/Au structure in solvents with different RI values (c) and refractive index sensitivity fitting curve (d).

Table 1
Comparison of sensor performance.

Sensing structure	Sensing materials	Refractive index range	Sensitivity (nm/RIU)	Metal film fabrication method use	Ref.
D-shape plastic optical fiber	Ag/MoS_2/Au film	1.35–1.3638	2473.37	vacuum thermal evaporation coating	[42]
Cylindrical coating	Ag/Au film/MoS_2 NSs	1.3318–1.3701	3061	magnetron sputtering coating	[20]
U-shape	MoS_2/Au film	1.3314–1.3623	6184.4	magnetron sputtering coating	[21]
Cylindrical coating	Ag film/MoS_2	1.333–1.373	3593	Magnetron Sputtering coating	[43]
Cylindrical coating	Au film/ $MoSe_2$	1.333–1.358	2793.36	vacuum sputtering coating	[17]
Cylindrical coating	Au film/$BaTiO_3$	1.3332–1.3710	2543	magnetron sputtering coating	[44]
Cylindrical coating	Au film	1.3329–1.3638	445.38–6214.31	ELP	this work
Cylindrical coating	MoS_2/AuNPs/Au film	1.3329–1.3638	678.85–7231.64	ELP	this work

change in resonance wavelength and the maximum change in reflectance of optical fiber SPR sensors with fiber/Au structure and fiber/MoS_2/AuNPs/Au structure prepared in the same and different batches respectively. Compared with six sensors prepared in the same batch, the resonance wavelength, the maximum change in resonance wavelength and reflectance were almost consistent, and the coefficients of variation of these values were in the range between 0.16 % and 4.22 %. Compared with these twelve sensors with the same structure and prepared in two batches, these values were also almost consistent.

4. Conclusions

An optical fiber SPR sensor with the MoS_2/AuNPs structure fabricated using ELP was developed in this study. A first PDA layer was deposited on the fiber core to absorb MoS_2 NSs via electrostatic interaction between the amion and imion groups of PDA and MoS_2 NSs. 1,2-ethanedithiol performed as linker to form MoS_2/AuNPs hybrid structure via thiol conjugation. A second PDA layer deposition on the optical fiber was used to absorb AuNPs as gold seeds to form an Au film using the ELP technique. The prepared sensor had refractive index sensitivity of 678.85–7231.64 nm/RIU in the range of 1.3329–1.3638, which was approximately 52.35 % and 16.37 % higher than that of conventional sensors without using MoS_2/AuNPs structure in the low refractive index range and high refractive index range respectively. The proposed ELP has proved useful for rapid, simple and economical fabrication of MoS_2/AuNPs hybrid structure enhanced optical fiber SPR sensor. Furthermore, this proposed sensor has huge potential in biomedical and chemical fields for accurate and precise detection.

CRediT authorship contribution statement

Yu Huang: Writing – review & editing, Writing – original draft, Supervision, Conceptualization. **Xiaomei Li:** Writing – original draft, Investigation. **Hua Zhang:** Investigation, Formal analysis. **Zhiguo Wu:** Investigation. **Rohan Weerasooriya:** Validation. **Xing Chen:** Resources. **Jiu Zhou:** Data curation. **Jiangling Wu:** Methodology. **Jianjiang Xue:** Visualization. **Junbo Wang:** Investigation. **Lei Feng:** Funding acquisition.

Declaration of competing interest

The authors declare that they have no known competing financial interests or personal relationships that could have appeared to influence the work reported in this paper.

Acknowledgements

This work was supported by Special Cooperation Project of Chinese Academy of Sciences and Hubei Province in 2024, the Project of Science and Technology Research Program of Chongqing Municipal Education Commission (Grant No. KJQN202200431), the Natural Science Foundation of Chongqing (grant no. cstc2020jcyj-msxmX0792 and CSTB2023NSCQ-MSX0175), Chongqing Medical Scientific Research Project (Joint Project of Chongqing Health Commission and Science and Technology Bureau, 2024QNXM037), Venture and Innovation Support Program for Chongqing Overseas Returnees (No. cx2023030), and the Talents Project of University-Town Hospital of Chongqing Medical University.

Appendix A. Supplementary material

Supplementary data to this article can be found online at https://doi.org/10.1016/j.optlastec.2024.112255.

Data availability

Data will be made available on request.

References

[1] A.K. Sharma, R. Jha, B.D. Gupta, Fiber-optic sensors based on surface plasmon resonance: a comprehensive review, IEEE Sens. J. 7 (8) (2007) 1118–1129, https://doi.org/10.1109/JSEN.2007.897946.
[2] P. Singh, S.P.R. Biosensors, Historical perspectives and current challenges, Sens. Actuators B 229 (2016) 110–130, https://doi.org/10.1016/j.snb.2016.01.118.
[3] Y.H. Huang, H.P. Ho, S.Y. Wu, S.K. Kong, W.W. Wong, P. Shum, Phase sensitive SPR sensor for wide dynamic range detection, Opt. Lett. 36 (20) (2011) 4092–4094, https://doi.org/10.1364/OL.36.004092.
[4] C. Caucheteur, T. Guo, J. Albert, Review of plasmonic fiber optic biochemical sensors: improving the limit of detection, Analytical and Bioanalytical Chemistry 407 (14) (2015) 3883–3897, https://doi.org/10.1007/s00216-014-8411-6.
[5] B. Peeters, D. Daems, T. Van der Donck, F. Delport, J. Lammertyn, Real-Time FO-SPR Monitoring of Solid-Phase DNAzyme Cleavage Activity for Cutting-Edge Biosensing, ACS Appl. Mater. Interfaces 11 (7) (2019) 6759–6768, https://doi.org/10.1021/acsami.8b18756.
[6] J. Lu, T. Van Stappen, D. Spasic, F. Delport, S. Vermeire, A. Gils, J. Lammertyn, Fiber optic-SPR platform for fast and sensitive infliximab detection in serum of inflammatory bowel disease patients, Biosens. Bioelectron. 79 (2016) 173–179, https://doi.org/10.1016/j.bios.2015.11.087.
[7] S.K. Gahlaut, A. Pathak, B.D. Gupta, J.P. Singh, Portable fiber-optic SPR platform for the detection of NS1-antigen for dengue diagnosis, Biosens. Bioelectron. 196 (2022) 113720, https://doi.org/10.1016/j.bios.2021.113720.
[8] D. Daems, W. Pfeifer, I. Rutten, B. Saccà, D. Spasic, J. Lammertyn, Three-Dimensional DNA Origami as Programmable Anchoring Points for Bioreceptors in Fiber Optic Surface Plasmon Resonance Biosensing, ACS Appl. Mater. Interfaces 10 (28) (2018) 23539–23547, https://doi.org/10.1021/acsami.8b04757.
[9] K. Vikas, R.K. Walia, Verma, Lossy mode resonance-based uniform core tapered fiber optic sensor for sensitivity enhancement, Commun. Theor. Phys. 72 (9) (2020) 095502, https://doi.org/10.1088/1572-9494/aba240.
[10] G.M. Shukla, N. Punjabi, T. Kundu, S. Mukherji, Optimization of Plasmonic U-Shaped Optical Fiber Sensor for Mercury Ions Detection Using Glucose Capped Silver Nanoparticles, IEEE Sens. J. 19 (9) (2019) 3224–3231, https://doi.org/10.1109/JSEN.2019.2893270.
[11] E. Klantsataya, P. Jia, H. Ebendorff-Heidepriem, T.M. Monro, A. François, Plasmonic Fiber Optic Refractometric Sensors: From Conventional Architectures to Recent Design Trends, Sensors 17 (1) (2017) 12, https://doi.org/10.3390/s17010012.
[12] R. Tabassum, R. Kant, Recent trends in surface plasmon resonance based fiber-optic gas sensors utilizing metal oxides and carbon nanomaterials as functional entities, Sens. Actuators B 310 (2020) 127813, https://doi.org/10.1016/j.snb.2020.127813.
[13] P. Thawany, A. Khanna, U.K. Tiwari, A. Deep, L-cysteine/MoS2 modified robust surface plasmon resonance optical fiber sensor for sensing of Ferritin and IgG, Sci. Rep. 13 (1) (2023) 5297, https://doi.org/10.1038/s41598-023-31152-3.
[14] W. Yang, Y. Cheng, M. Jiang, S. Jiang, R. Liu, J. Lu, L. Du, P. Li, C. Wang, Design and fabrication of an ultra-sensitive Ta2C MXene/Au-coated tilted grating sensor, Sens. Actuators B 369 (2022) 132391, https://doi.org/10.1016/j.snb.2022.132391.
[15] J. Tan, Y. Chen, J. He, L.G. Occhipinti, Z. Wang, X. Zhou, Two-dimensional material-enhanced surface plasmon resonance for antibiotic sensing, J. Hazard. Mater. 455 (2023) 131644, https://doi.org/10.1016/j.jhazmat.2023.131644.
[16] W. Wei, J. Nong, Y. Zhu, G. Zhang, N. Wang, S. Luo, N. Chen, G. Lan, C.-J. Chuang, Y. Huang, Graphene/Au-Enhanced Plastic Clad Silica Fiber Optic Surface Plasmon Resonance Sensor, Plasmonics 13 (2) (2018) 483–491, https://doi.org/10.1007/s11468-017-0534-0.
[17] K. Liu, J. Zhang, J. Jiang, T. Xu, S. Wang, P. Chang, Z. Zhang, J. Ma, T. Liu, MoSe2-Au Based Sensitivity Enhanced Optical Fiber Surface Plasmon Resonance Biosensor for Detection of Goat-Anti-Rabbit IgG, IEEE Access 8 (2020) 660–668, https://doi.org/10.1109/ACCESS.2019.2961751.
[18] A.K. Mishra, S.K. Mishra, R.K. Verma, Graphene and Beyond Graphene MoS2: A New Window in Surface-Plasmon-Resonance-Based Fiber Optic Sensing, J. Phys. Chem. C 120 (5) (2016) 2893–2900, https://doi.org/10.1021/acs.jpcc.5b08955.
[19] S. Kaushik, U.K. Tiwari, S.S. Pal, R.K. Sinha, Rapid detection of Escherichia coli using fiber optic surface plasmon resonance immunosensor based on biofunctionalized Molybdenum disulfide (MoS2) nanosheets, Biosens. Bioelectron. 126 (2019) 501–509, https://doi.org/10.1016/j.bios.2018.11.006.
[20] Q. Wang, X. Jiang, L.-Y. Niu, X.-C. Fan, Enhanced sensitivity of bimetallic optical fiber SPR sensor based on MoS2 nanosheets, Opt. Lasers Eng. 128 (2020) 105997, https://doi.org/10.1016/j.optlaseng.2019.105997.
[21] H. Song, Q. Wang, W.-M. Zhao, A novel SPR sensor sensitivity-enhancing method for immunoassay by inserting MoS2 nanosheets between metal film and fiber, Opt. Lasers Eng. 132 (2020) 106135, https://doi.org/10.1016/j.optlaseng.2020.106135.
[22] Z. Hou, N.L. Abbott, P. Stroeve, Electroless Gold as a Substrate for Self-Assembled Monolayers, Langmuir 14 (12) (1998) 3287–3297, https://doi.org/10.1021/la971327p.
[23] Y. Lei, H. Chen, H. Dai, Z. Zeng, Y. Lin, F. Zhou, D. Pang, Electroless-plated gold films for sensitive surface plasmon resonance detection of white spot syndrome virus, Biosens. Bioelectron. 23 (7) (2008) 1200–1207, https://doi.org/10.1016/j.bios.2007.10.004.
[24] A. Lahiri, S.I. Kobayashi, Electroless deposition of gold on silicon and its potential applications: review, Surf. Eng. 32 (5) (2016) 321–337, https://doi.org/10.1179/1743294415Y.0000000060.
[25] A. Shoji, M. Nakajima, K. Morioka, E. Fujimori, T. Umemura, A. Yanagida, A. Hemmi, K. Uchiyama, H. Nakajima, Development of a surface plasmon resonance sensor using an optical fiber prepared by electroless displacement gold plating and its application to immunoassay, Talanta 240 (2022) 123162, https://doi.org/10.1016/j.talanta.2021.123162.
[26] M. Loyez, C. Ribaut, C. Caucheteur, R. Wattiez, Functionalized gold electroless-plated optical fiber gratings for reliable surface biosensing, Sens. Actuators B 280 (2019) 54–61, https://doi.org/10.1016/j.snb.2018.09.115.
[27] Y. Huang, X. Pu, H. Qian, C.-J. Chuang, S. Dong, J. Wu, J. Xue, W. Cheng, S. Ding, S. Li, Optical fiber surface plasmon resonance sensor using electroless-plated gold film for thrombin detection, Anal. Bioanal. Chem. 416 (6) (2024) 1469–1483, https://doi.org/10.1007/s00216-024-05150-x.
[28] C.G. Bailey, M.D. Nothling, L.L. Fillbrook, Y. Vo, J.E. Beves, D.R. McCamey, M. H. Stenzel, Polydopamine as a visible-light photosensitiser for photoinitiated polymerisation, Angew. Chem. Int. Ed. 62 (20) (2023), https://doi.org/10.1002/anie.202301678.
[29] N.F. Della Vecchia, R. Avolio, M. Alfè, M.E. Errico, A. Napolitano, M. d'Ischia, Building-Block Diversity in Polydopamine Underpins a Multifunctional Eumelanin-Type Platform Tunable Through a Quinone Control Point, Advanced Functional Materials 23(10) (2013) 1331-1340. Doi: 10.1002/adfm.201202127.
[30] S. Shi, L. Wang, A. Wang, R. Huang, L. Ding, R. Su, W. Qi, Z. He, Bioinspired fabrication of optical fiber SPR sensors for immunoassays using polydopamine-accelerated electroless plating, J. Mater. Chem. C 4 (32) (2016) 7554–7562, https://doi.org/10.1039/C6TC02149B.
[31] Y. Xie, Y. Huang, D. Tang, H. Cui, H. Cao, A competitive colorimetric chloramphenicol assay based on the non-cross-linking deaggregation of gold nanoparticles coated with a polyadenine-modified aptamer, Microchim. Acta 185 (12) (2018) 534, https://doi.org/10.1007/s00604-018-3067-0.
[32] Y. Huang, S. Li, C. Liu, L. Chen, H. Qian, H.-P. Ho, J. Wu, J. Wu, X. Pu, One-step competitive assay for detection of thrombin via disassembly of diblock oligonucleotide functionalised nanogold aggregates, Sens. Actuators B 376 (2023) 133032, https://doi.org/10.1016/j.snb.2022.133032.
[33] J. Li, W. Yun, H. Zhang, L. Chen, H.-P. Ho, X. Pu, Y. Huang, Y. Shen, H. Cao, MoS2 nanosheets based label-free colorimetric aptasensor for Escherichia coli O157: H7

detection, Colloids and Surfaces a: Physicochemical and Engineering Aspects 674 (2023) 131955, https://doi.org/10.1016/j.colsurfa.2023.131955.
[34] X. Hai, K. Chang, H. Pang, M. Li, P. Li, H. Liu, L. Shi, J. Ye, Engineering the Edges of MoS2 (WS2) Crystals for Direct Exfoliation into Monolayers in Polar Micromolecular Solvents, J. Am. Chem. Soc. 138 (45) (2016) 14962–14969, https://doi.org/10.1021/jacs.6b08096.
[35] M. Velický, M.A. Bissett, C.R. Woods, P.S. Toth, T. Georgiou, I.A. Kinloch, K. S. Novoselov, R.A.W. Dryfe, Photoelectrochemistry of Pristine Mono- and Few-Layer MoS2, Nano Lett. 16 (3) (2016) 2023–2032, https://doi.org/10.1021/acs.nanolett.5b05317.
[36] B.L. Li, H.L. Zou, L. Lu, Y. Yang, J.L. Lei, H.Q. Luo, N.B. Li, Size-Dependent Optical Absorption of Layered MoS2 and DNA Oligonucleotides Induced Dispersion Behavior for Label-Free Detection of Single-Nucleotide Polymorphism, Adv. Funct. Mater. 25 (23) (2015) 3541–3550, https://doi.org/10.1002/adfm.201500180.
[37] Q. Ding, K.J. Czech, Y. Zhao, J. Zhai, R.J. Hamers, J.C. Wright, S. Jin, Basal-Plane Ligand Functionalization on Semiconducting 2H-MoS2 Monolayers, ACS Appl. Mater. Interfaces 9 (14) (2017) 12734–12742, https://doi.org/10.1021/acsami.7b01262.
[38] S.S. Singha, S. Mondal, T.S. Bhattacharya, L. Das, K. Sen, B. Satpati, K. Das, A. Singha, Au nanoparticles functionalized 3D-MoS2 nanoflower: An efficient SERS matrix for biomolecule sensing, Biosens. Bioelectron. 119 (2018) 10–17, https://doi.org/10.1016/j.bios.2018.07.061.
[39] S.-Y. Cho, H.-J. Koh, H.-W. Yoo, J.-S. Kim, H.-T. Jung, Tunable Volatile-Organic-Compound Sensor by Using Au Nanoparticle Incorporation on MoS2, ACS Sensors 2 (1) (2017) 183–189, https://doi.org/10.1021/acssensors.6b00801.
[40] J. Homola, Surface Plasmon Resonance Sensors for Detection of Chemical and Biological Species, Chem. Rev. 108 (2) (2008) 462–493, https://doi.org/10.1021/cr068107d.
[41] J. Jing, K. Liu, J. Jiang, T. Xu, S. Wang, T. Liu, Highly sensitive and stable probe refractometer based on configurable plasmonic resonance with nano-modified fiber core, Opto-Electronic Advances 6 (6) (2023) 220072, https://doi.org/10.29026/oea.2023.220072.
[42] B. Man, G. Wang, Z. Li, S. Xu, C. Li, J. Yu, C. Zhang, X. Zhao, MoS2-spaced bimetal composite structure as SERS-SPR sensor for glucose detection, J. Alloy. Compd. 902 (2022) 163789, https://doi.org/10.1016/j.jallcom.2022.163789.
[43] L. Li, L. Zhao, X. Zong, Y. Li, P. Li, Y. Liu, Transition metal dichalcogenides boost the performance of optical fiber SPR sensors, Opt. Commun. 520 (2022) 128485, https://doi.org/10.1016/j.optcom.2022.128485.
[44] Q. Wang, L.-Y. Niu, J.-Y. Jing, W.-M. Zhao, Barium titanate film based fiber optic surface plasmon sensor with high sensitivity, Opt. Laser Technol. 124 (2020) 105899, https://doi.org/10.1016/j.optlastec.2019.105899.